Energy 333 (2025) 137379

Contents lists available at ScienceDirect

Energy

journal homepage: www.elsevier.com/locate/energy

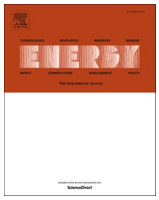

Development of a reduced-order dynamic model for large-scale seasonal thermal energy storage applications

Michael Bayer [a,b], Curtis Meister [a], Philipp Schuetz [a], Willy Villasmil [a,*], Heimo Walter [b], Abdulrahman Dahash [c]

[a] School of Engineering and Architecture, Lucerne University of Applied Sciences and Arts, 6048, Horw, Switzerland
[b] Institute for Energy Systems and Thermodynamics, TU Wien, Getreidemarkt 9, 1060, Vienna, Austria
[c] Sustainable Thermal Energy Systems, Center for Energy, AIT Austrian Institute of Technology GmbH, 1210, Vienna, Austria

ARTICLE INFO

Keywords:
Reduced-order model
Seasonal thermal energy storage
pit thermal energy storage
Modelica model
DePlaTES COMSOL
Energy system simulations

ABSTRACT

This study introduces an efficient simulation model for large-scale pit seasonal thermal energy storage (PTES) applications, designed to retain accuracy while significantly reducing computational demands. Being implemented in Modelica/Dymola, the reduced-order model is compared against an experimentally validated COMSOL Multiphysics simulation model based on key performance indicators including energy balance, thermal losses, temperature stratification and computational time. Energy balances of both models show good agreement, with deviations of less than 6 % in terms of charged energy and under 5 % in discharged energy. Total thermal losses align closely, with discrepancy below 2 %, underscoring the model's reliability. Temperature stratification analysis reveals strong alignment of both models under idle conditions, especially in the upper layers of the storage. During dynamic charging and discharging phases, minor discrepancies are observed, with root mean square error values ranging from 1.2 K in the upper layers to 2.4 K at the bottom. Additionally, the reduced-order model demonstrates a substantial reduction in computational time, making it up to 98 % faster than the COMSOL model. The model is therefore established as a highly efficient yet accurate tool for large-scale sTES simulations, particularly suited for iterative system design, optimization processes, and real-time control.

Nomenclature

Latin Symbols		
A	area	m^2
a, b	top dimensions of storage	m
a_{seg} , b_{seg}	top dimensions of segment	m
a_1 , b_1	bottom dimensions of storage	m
a_{1seg} , b_{1seg}	bottom dimensions of segment	m
C	heat capacitance	J/K
c_p	specific heat capacity	J/(kg·K)
E	energy	J
H	height	m
$\dot{H}$	enthalpy flow	W
h	specific enthalpy	J/kg
k_{bou}	proportionality constant for buoyancy calculation	
Δy_i	height of ground element	m
$\dot{m}$	mass flow rate	kg/s
Q	thermal energy	J
$\dot{Q}$	heat flow	W

(*continued on next column*)

(*continued*)

R	thermal resistance	K/W
$RMSE$	root mean square error of temperature	K
T	temperature	K
t	time	s
U	overall heat transfer coefficient	W/(m²·K)
V	volume	m^3
$\dot{V}$	volumetric flow rate	m^3/s
ΔT	temperature difference	K
Δx_i	width of ground element	m
Δz_i	distance between fluid nodes	m
Greek Symbols		
α_c	convective heat transfer coefficient	W/(m²·K)
β	slope angle	°
λ	thermal conductivity	W/(m·K)
ρ	density	kg/m^3
τ	mixing time constant	s
θ	temperature	°C

(*continued on next page*)

This article is part of a special issue entitled: SESAAU2024 published in Energy.

* Corresponding author.
E-mail address: willy.villasmil@hslu.ch (W. Villasmil).

https://doi.org/10.1016/j.energy.2025.137379
Received 20 December 2024; Received in revised form 23 June 2025; Accepted 1 July 2025
Available online 2 July 2025

(*continued*)

Subscripts	
bot	bottom
buo	buoyancy
ch	charge
dc	discharge
ext	external
flow	flow
g	ground
i	segment index of storage
i–1	segment above
i+1	segment below
loss	heat loss
left	left
right	right
seg	segment of the storage
side	side
sTES	seasonal thermal energy storage
top	top
tot	total
wall,i	wall of segment
W	water
[x,y]	index of ground element
Abbreviations	
API	application programming interfaces
CFD	computational fluid dynamics
DH	district heating
ESS	energy system simulation
FE	finite element
FMU	functional mock-up unit
KPI	key performance indicator
PTES	pit thermal energy storage
RC	resistance capacitance model
RES	renewable energy sources
ROM	reduced-order model
sTES	seasonal thermal energy storage
TES	thermal energy storage
TTES	tank thermal energy storage

1. Introduction

In recent decades, the integration of renewable energy sources (RES) into national energy systems has become a strategic focus to combat climate change and reduce dependency on fossil fuels. The European Union, for instance, has set ambitious goals to lower carbon emissions by 80 % by 2050. This will require transformative changes across all sectors, particularly heating and cooling, which account for a substantial share of overall emissions in Europe – around 40 % [1–4]. Decarbonizing this sector is critical to achieving these targets [4]. This shift toward renewable-based heating systems, such as district heating (DH) and solar district heating, has spurred interest in seasonal thermal energy storage (sTES) systems, which can store energy for long periods, balancing supply-demand mismatches due to seasonal variation in both RES availability and heat demand [5].

Thermal energy storage (TES) systems, particularly large-scale solutions like sTES, play a central role in maximizing the utility of RES. These systems absorb surplus energy from sources like solar thermal arrays during periods of high availability and store it for later use during periods of high demand in colder months [6–8]. Thus, sTES enhances system flexibility, enabling the increased integration of RESs and improving overall system efficiency. Moreover, sTES can play a crucial role in sector coupling when coupled to power-to-heat technologies (e.g. heat pumps) as it helps to balance the power grid. Among TES technologies, sensible heat storage systems, such as tank thermal energy storage (TTES) and pit thermal energy storage (PTES), have shown promise for large-scale DH applications. For example, the operational experience of the Dronninglund DH plant in Denmark (among many other such plants in Denmark) highlights the potential of sTES to significantly reduce fossil fuel consumption in DH systems, utilizing a PTES to achieve a solar fraction above 40 % [9,10].

Despite this experience and existing know-how, the design and construction of large-scale sTES systems remains a complex task. As such, it requires careful consideration of factors like storage volume, geometry, construction type, and insulation materials to optimize both energy efficiency and economic feasibility [3]. Environmental factors, particularly subsurface conditions like groundwater quality, add further layers of complexity to the planning process, as large underground storage systems must minimize thermal losses and mitigate potential environmental impacts [5]. Moreover, effective sTES implementation often involves the challenge of coupling with low-temperature DH networks to enhance operational efficiencies and the capacity to integrate diverse renewable heat sources [11].

Consequently, numerical modeling and dynamic simulation have become vital instruments for evaluating and optimizing sTES system designs and ensuring their reliable and optimal operation. Detailed high-fidelity models, such as those built in COMSOL Multiphysics, provide insights via multi-physics simulations that capture the sophisticated thermal and hydraulic behaviors within sTES systems. However, such models are computationally intensive, which can limit their practicality for iterative system design, optimization scenarios [12] or real-time control. In response to this challenge, recent research has emphasized the importance of developing reduced-order models (ROM) that maintain accuracy while reducing computational demands. These ROMs are particularly useful in the predesign stages, where iterative simulations are often required to explore different configurations and operational strategies [13,14].

1.1. Planning and construction of large-scale sTES

The planning of large-scale sTES systems, particularly those exceeding 50,000 m^3, presents a complex challenge [15]. This complexity arises due to the need to address multiple interrelated decisions, which often evolve during later phases of the planning process. Critical considerations that emerge during sTES planning include.

a) What is the optimal storage volume for integration within a renewable-powered district heating system?
b) What construction type is most appropriate for the thermal energy storage system? (e.g., freestanding, partially buried, fully buried)
c) What is the optimal geometry of the TES? (e.g., cylindrical tank, cuboid tank, cone pit, pyramid pit, hybrid design)

These initial questions expand as technical decisions regarding the system's layout are made, subsequently leading to further considerations of economic feasibility. Environmental factors, particularly those concerning subsurface conditions such as groundwater quality, can further increase the complexity of the planning process, making it highly sophisticated.

The interdependencies among the various factors, as illustrated in Fig. 1, underscore the importance of TES simulations. Given that large-scale TES systems are capital-intensive, modeling becomes necessary in ensuring both economic feasibility and efficiency of the system design [16]. The modeling process not only aids in optimizing the system layout but also helps bridge knowledge gaps, providing a deeper understanding of system performance.

TES modeling, therefore, plays a crucial role in the planning and development of sustainable energy systems. The modeling approach can be adapted to different levels of complexity, depending on the objectives of the analysis. Typically, TES modeling follows a structured process, encompassing stages such as pre-design, detailed design, technology integration, and ultimately, evaluation and optimization.

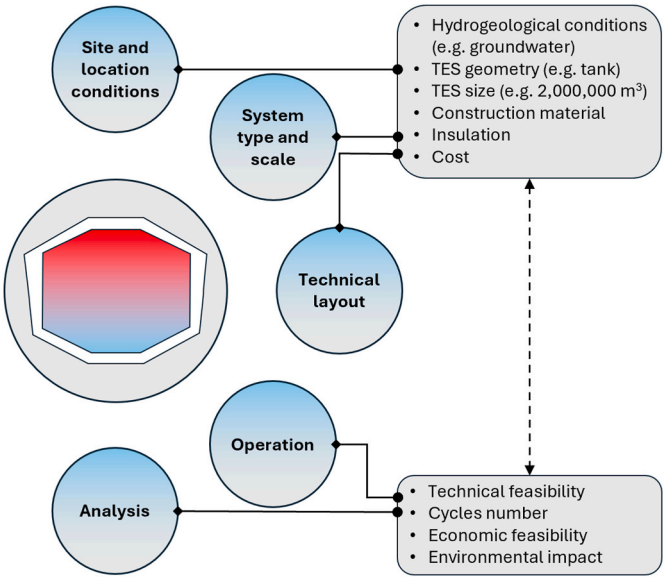

Fig. 1. *An exemplary sketch illustrating major dimensions and resulting specific aspects influencing the planning and construction of underground TES and its economic feasibility (reproduced from* Ref. [17]).

1.2. Modeling and simulation of large-scale sTES

Dahash et al. [18] proposed a sequential hierarchy for simulating large-scale thermal energy storage systems as illustrated in Fig. 2. The process starts with **preliminary design**, using pre-design tools to assess the feasibility of integrating large scale sTES into district heating systems. Following this, a more detailed simulation model is developed, accounting for multi-physics aspects such as fluid flow, heat and mass transfer. This model enables a comprehensive sTES design, including components such as the water domain, thermal insulation, and cover.

Next, in the **integration phase**, interactions between the sTES and other technologies are evaluated using integration tools. Simulations generate outputs that are analyzed for feasibility. If needed, the process advances to an **optimization phase** to refine the design and achieve optimal performance.

Additionally, **computation time** is a key factor, influenced by the level of detail, number of components, and simulation timestep. To position different modeling approaches used in thermal energy storage literature, Fig. 3 provides a conceptual diagram showing the trade-offs between component complexity, system scope, and temporal resolution. Component complexity refers to the level of physical detail used in representing individual subcomponents, including spatial discretization. System complexity reflects the number of coupled subcomponents (e.g. heat pump, thermal energy storage, boiler) or processes (e.g. heat transfer, mass transfer, transport of species), while simulation time step describes the temporal granularity. Planners must align the goals of the sTES analysis with the appropriate simulation tools and computational settings to ensure suitable efficiency and accuracy [12].

The importance of thermo-hydraulic simulations in accurately predicting the behavior of sTES systems is well-established, though these

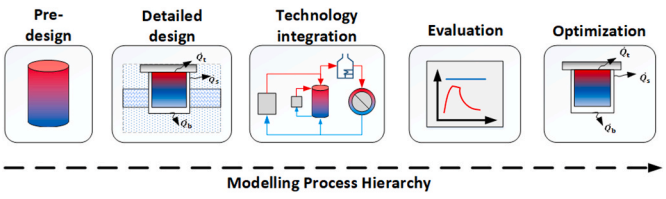

Fig. 2. An example hierarchy for modeling process of large-scale sTES in DH systems (reproduced from Ref. [47].).

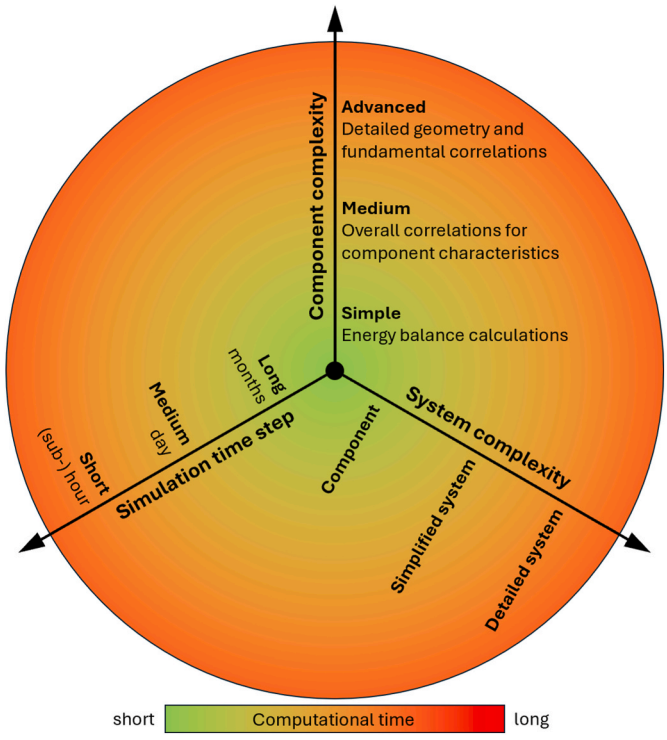

Fig. 3. *Computation time for sTES simulations (reproduced from* Ref. [16]).

simulations are complex due to their multi-physical nature. To address this, various tools are available, each suited for specific applications, and can be categorized as follows.

a) **Energy System Simulations (ESS)**: Tools like TRNSYS, Modelica/Dymola, IDA ICE, and MATLAB/Simulink typically focus on system-level energy dynamics.
b) **Building Physics Heat and Mass Transfer**: Tools such as WUFI Pro and Delphin simulate heat and moisture transfer through building envelopes.
c) **Computational Fluid Dynamics (CFD)**: ANSYS Fluent, OpenFOAM, and STAR-CCM + model detailed fluid flow behavior.
d) **Multiphysics Tools**: COMSOL Multiphysics handles diverse physical phenomena like heat transfer, fluid flow, and structural mechanics.

Key features to distinguish these tools include.

1. **Spatial discretization method**: Tools may use finite difference, finite volume, or finite element (FE) schemes based on the application's complexity.
2. **Level of detail/considered physical effects**: Models range from 0-D and 1-D (common in ESS tools for faster simulations) to 3-D (used in CFD for detailed analysis).
3. **Temporal discretization**: Varies by tool depending on the specific simulation needs.

Therefore, the optimal selection of the appropriate simulation tool depends on the goals, level of detail, and phenomena being modeled. Different tools excel in different areas, making the right choice crucial for efficient and accurate sTES system planning. Consequently, this paper will focus on the tools within the categories of energy system simulations, particularly TRNSYS and Modelica/Dymola, and multi-physics tools (i.e. COMSOL Multiphysics).

1.2.1. Energy system tools

The following section reviews modeling approaches for large-scale

seasonal thermal energy storage systems with a focus on the underlying physical complexity, dimensional assumptions, and the inclusion of influencing parameters such as geometry, operational behavior, and ground coupling. Although the models are grouped according to their implementation environments (e.g., TRNSYS, Modelica, COMSOL), this classification is used as a proxy for the associated modeling approaches, which range from simplified lumped-element methods to high-resolution, multiphysics simulations.

1.2.1.1. TRNSYS. In TRNSYS [19], several models have been developed to simulate sTES dynamics, ranging from 1-D to 3-D models. The XST model (Type 342) was one of the earliest, designed for cylindrical tanks [20]. This model allows simulations of cylindrical tanks only, which means that the interfacing between the underground storage and the surrounding soil is a vertical line and cannot be represented with a slope. Besides, this model suffers from a major drawback that the number of ports is limited to one port at the top and one port at the bottom. Therefore, the ICEPIT model (Type 343) was developed, accommodating additional geometries like cones and other storage media such as gravel-water mixtures [18]. Yet, this model cannot capture or simulate a truncated pyramid in its actual shape, it has to approximate the shape with a cone. Accordingly, this model allows a sloped interface between the storage and the ground. However, the neighboring soil cells are discretized into a triangular grid instead of quadrilateral leading to some major computational throwbacks (e.g., miscalculation due to misallocation of cells, longer simulation times). While models like Type 534 can simulate PTES [21], their suitability for large-scale systems is sometimes questioned as they cannot capture the correct geometry of PTES and are more applicable for residential hot water tanks.

Bai et al. [22] introduced the UGSTS model, a simplified 1-D simulation model for underground sTES, later extended for sloped-wall designs [23]. However, the model still has limitations in representing the envelope components of sTES systems as it simulates a vertical-wall, cylindrical TES with approximation to sloped-walls pit. Xie et al. [24] expanded ICEPIT to include 16 ports but kept the focus on specific geometries, like cones. More recent advancements, such as Type 1300 and Type 1322, simulate sloped-wall systems with greater accuracy, representing complex shapes like truncated pyramids [25,26]. However, these recent models simulate the PTES with ground interaction by only using one quarter, assuming two symmetrical planes. Despite the effectiveness of this approach, this can lead to major issues when groundwater flow is considered. It is worth mentioning that all models in TRNSYS use finite difference discretization.

1.2.1.2. Modelica/Dymola. Dymola, a widely used tool for energy system simulations, stands out for its use of Modelica, an open-source, equation-based language ideal for modeling dynamic, multi-domain systems. This makes it highly flexible, with extensive free libraries (e.g., Buildings [27], IDEAS [28], AixLib [29], BuildingSystems [30]) and commercial libraries (e.g., TIL [31–33], TIL Media [34], ClaRa/ClaRa^{+} [35]), allowing for optimal system planning.

The Buildings library [27], commonly used in academia and industry, includes 1-D stratified storage models suitable for small-scale energy systems. Its *StratifiedEnhanced* model uses a first-order upwind finite volume scheme, but reduces numerical diffusion using an approximation of a third-order upwind scheme. While these models can be extended and calibrated, their application for large-scale underground TES systems remains limited. They often lack features like diverse geometries (e.g., cones, pyramids) and suitable soil models for subsurface storage.

Despite these limitations, Köfinger et al. [36] used the Buildings library for a simulation-driven assessment of a large-scale TES system in Linz, Austria, aiming to maximize waste heat utilization. However, the model's applicability for large PTES was questioned. Dahash et al. [37] extended the stratified storage model for large-scale TES by improving buoyancy functions with more physics-based coefficients, side heat ports, and integrating a 2-D soil model. This version allowed for more detailed settings, such as insulation properties and temperature initialization, and showed improved accuracy in large-scale buried tank simulations.

Reisenbichler et al. [38] further developed a toolkit based on the Buildings library for large-scale TES systems, including soil models and customization options for insulation. Their model, calibrated against the Dronninglund PTES, showed good agreement with measured data, although some discrepancies (e.g., 12 % error in thermal losses) were attributed to geometric differences, as the model was designed for cylindrical tanks.

Most recently, Formhals et al. [13] created an enhanced PTES model in Modelica (MoSDH library). The model was compared to a more detailed and validated COMSOL model (later this model was renamed as DePlaTES, which is serving as a benchmark for this study as well). While the MoSDH model showed good accuracy for early-stage design (2–13 % deviation in annual charge/discharge), it exhibits some structural limitations. Specifically, it supports only fixed geometries, based on multiple cylindrical segments, leading to an approximated slope of the PTES. Additionally, the model has a predefined pit shape and embedded embankment, with limited flexibility for adapting inlet/outlet configurations (three fixed ports, with only one adjustable without major code changes). The model is not fully compatible with the Modelica Standard Library, and due to computational constraints from complex ground meshing, it is limited to ~20 tank layers — insufficient for accurately capturing thermal stratification. Additionally, the cylindrical ground domain restricts the ability to apply spatially varying boundary conditions, such as when multiple storage units are co-located. These constraints reduce its usability for broader parametric studies and layout-dependent scenarios.

1.2.1.3. MATLAB/Simulink. Bott et al. [39] developed a numerical model for sTES in Simulink using Simscape. The model, based on finite difference discretization, simulates various storage mediums like water and water-gravel. It supports TES configurations with vertical walls (e.g., tanks, cuboids) and includes detailed layers for sidewalls and bottoms (e.g., insulation, concrete) with customizable thermophysical properties. The model underwent a plausibility test and was compared with a validated model from the CARNOT toolbox [40], focusing on a 4000 m^3 cuboid TES. Despite reasonable agreement, some discrepancies in temperature profiles were noted due to model differences. The CARNOT toolbox, which primarily supports cylindrical stratified storage models, was adapted by adjusting *UA* values to approximate a cuboid geometry, while the Simscape model did not consider natural convection. These limitations were acknowledged as areas for future refinement.

1.2.2. Multi-physics tools

Large-scale TES systems are thermo-hydraulic systems influenced by various physical phenomena, including conduction, convection, mass transfer, and groundwater flow. Multi-physics simulation tools are essential for effectively addressing these complexities. **COMSOL Multiphysics** is particularly valuable for developing FE models that integrate the diverse physical characteristics of large-scale TES systems.

Dahash et al. [41] developed a flexible FE model adaptable to different TES shapes, including cylinders, cones, pyramids, and cuboids. This model can represent the TES envelope — top covers, sidewalls, and bottoms — using either individual thermophysical properties or a lumped equivalent value. By utilizing axisymmetry, the model efficiently simulates cylinders and cones surrounded by a 2-D soil domain, reducing computational requirements. For pyramids or cuboids, a 3-D soil model is employed. Validation against data from the Dronninglund PTES for 2015 showed agreement between measured and simulated results (deviation below 2 %), with conical designs achieving shorter simulation times compared to pyramidal configurations [12].

Subsequent research [42] enhanced the model to include groundwater simulations for areas designated for large-scale TES construction. Cross-comparisons with FEFLOW [43] demonstrated strong temperature correlations in the subsurface, affirming the model's utility in detailed planning. Another effort [44] aimed to extend the model for simplified DH system simulations, integrating various heat sources and predefined load profiles, though it does not dynamically simulate the DH network.

Additionally, Salvestroni et al. [45] explored a solar-assisted DH system with sTES using numerical simulations. The system was divided into three parts, each simulated with distinct tools. Initially, the building's heating demand was modeled using Thermal Analysis Software (TAS, [46]) to predict energy demand requirements, providing boundary conditions for the solar DH system simulation in TRNSYS. This study incorporated TES simulations in TRNSYS, with the TES temperature profile feeding into a separate large-scale TES model in COMSOL Multiphysics to accurately predict thermal losses. This iterative process continued until the deviation between TRNSYS and COMSOL results was less than 1 %. However, it is important to note that this model was not validated, and the process was considered unnecessarily lengthy.

1.3. Contribution of this work

This study contributes to this growing body of research by developing a reduced order sTES model in Modelica/Dymola and validating it against a detailed COMSOL model. Our approach focuses on balancing accuracy and computational efficiency, targeting key performance metrics such as the energy balance, thermal losses, temperature stratification, and computational time. Building upon a stratified tank model, the proposed ROM has been tailored for broad applicability in district heating contexts. Key enhancements include flexible geometric definitions (cylindrical, conical, truncated pyramids), user-configurable inlet and outlet positions, and full compatibility with the Modelica Standard Library. Additionally, the model integrates a configurable ground domain that allows spatially variable boundary conditions and inhomogeneous multilayer soil. While such features are generally possible in finite difference frameworks, they are often missing or hardcoded in many ROM implementations. The model supports fine spatial discretization, such as hundreds of tank segments, while maintaining computational efficiency. The model is designed for practical application in renewable-powered DH systems, offering a tool that can support early-phase planning and help streamline the integration of sTES in large-scale renewable heating networks.

2. Materials and methods

The methodology involves two phases: model development and calibration. First, a validated detailed COMSOL model [12] is used as the reference for simulating various scenarios. The reduced-order model is then developed and calibrated to replicate the behavior of the detailed model. Finally, comparisons are made between the two models in terms of key performance indicators (KPIs) such as the energy balance, thermal losses, temperature stratification, and computational time. Fig. 4 illustrates the workflow and structure of the **system modeling process** for the sTES system, emphasizing both the detailed model and the reduced-order model components. FMU integration offers an outlook for extending the ROM's usability within broader energy simulation platforms. The diagram is divided into several sections to highlight the different stages and aspects of the modeling approach.

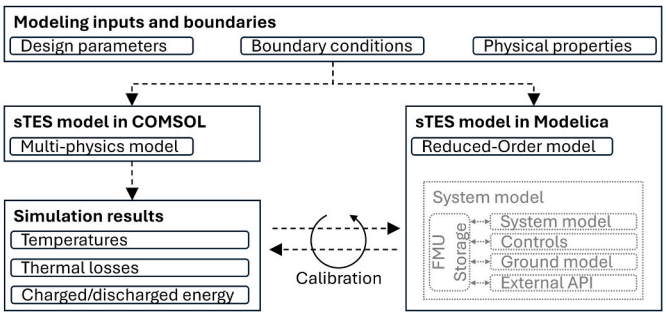

Fig. 4. Overview of the modeling process and model calibration.

2.1. Multi-physics, detailed, numerical model of large-scale sTES

COMSOL Multiphysics is an effective tool for modeling and analyzing the complex multi-physical challenges associated with various geometrical TES configurations, such as pits and tanks. The software utilizes axisymmetric features, allowing users to simulate circular cross-sectional geometries in a 2-D environment, which significantly reduces computation time. However, addressing issues involving groundwater flow or non-circular cross-sections requires the use of a 3-D simulation environment. Fig. 5 illustrates the structure of *DePlaTES*, a comprehensive planning toolkit designed for large-scale sTES systems, originally developed by Dahash et al. [12]. It was validated by using experimental data from the 60,000 m^3 Dronninglund PIT [12]. The toolkit consists of two main models: one for sTES itself and another for the subsurface environment surrounding the sTES. *DePlaTES* provides users with several options for sTES, including construction types (partially or fully buried), geometries (tank, shallow pit, cavern), storage media (water, gravel, sand), number of charging/discharging ports, and thermal insulation materials. Additionally, the subsurface model offers further flexibility, allowing users to account for groundwater presence and flow, various soil types, and other parameters. Users can specify the location of the sTES application, after which the tool automatically loads reference weather data for that area; alternatively, users can import measured data if available. In this study, the validated model

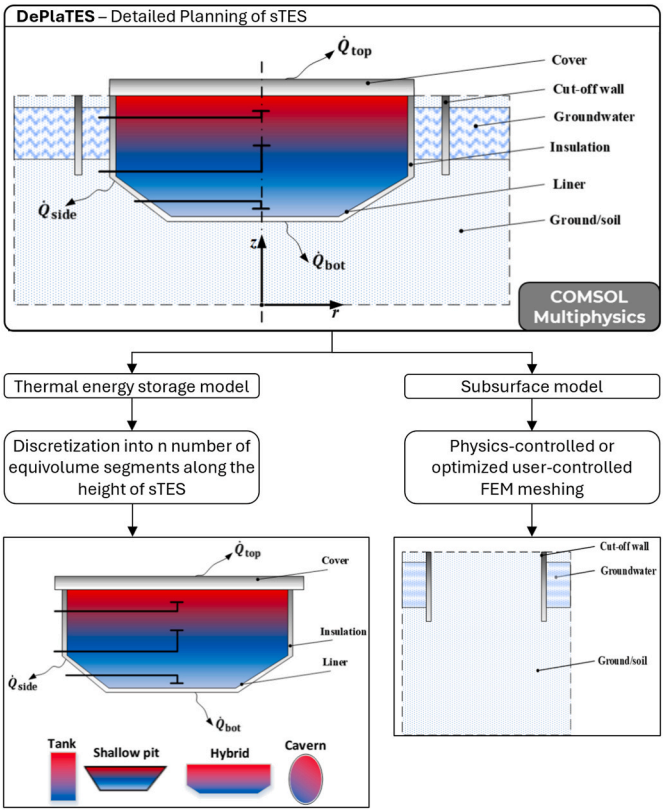

Fig. 5. Structure of DePlaTES as implemented in COMSOL Multiphysics. DePlaTES encompasses two sub models: one considers large-scale TES (left-hand side) and the other focuses on the subsurface (right-hand side).

within DePlaTES toolkit is used as the high-fidelity reference to assess the accuracy of the proposed ROM. The validation in Ref. [12] includes comparison of thermal losses, stratification, and operational dynamics, confirming its suitability for use as a benchmark.

2.2. Modelling inputs and boundaries

In this study, PTES systems are modeled as truncated pyramid shapes with square cross-sections. Five different sizes, ranging from 20,000 up to 200,000 m^3, were simulated to assess the effect of storage volume on system and model performance. The specific dimensions for the different sTES sizes are summarized in Table 1. The top and bottom surfaces of the storage are defined by side lengths a, b and a_1, b_1, respectively. The height of the sTES is denoted by H, and the side slope angle (β) is set at 30° for all sizes. In the model, diffusers are located 0.5 m below the sTES lid and 0.5 m above the bottom of the sTES.

To ensure model accuracy while avoiding unnecessary time-consuming simulations, simplified temperature and flow rate profiles are used as model inputs. These profiles focus solely on the sTES system, excluding any external generation or consumption units. By concentrating on component modeling within the sTES, this study addresses the dynamic behavior of the sTES system under different operational conditions. As illustrated in Fig. 6, the periodic operation of the system—charging, storing, discharging, and idle phase—follows an idealized annual storage cycle. The charging phase involves injecting hot water at 95 °C into the top of the sTES, while colder water is extracted from the bottom (see Fig. 6a). During discharge, the reverse occurs: hot water is drawn from the top, and cooler water (at 55 °C) is injected into the bottom. These temperatures determine the behavior of the charging and discharging cycles of the system. Fig. 6b illustrates the inlet flow rate profile over the course of one annual cycle. The flow rate is set to achieve one full sTES turnover of its volume during the 90 days of charging and discharging phases, depending on storage size. Positive values indicate charging phases, while negative values reflect discharging phases. Additionally, the different thermo-physical properties and the heat transfer coefficients used for the materials in the modeling of the sTES are listed in Table 2. The same parameters are used in both the COMSOL and reduced-order models. While the thermal conductivity of water varies with temperature, using a constant value introduces negligible error at the control volume scale. Similarly, fixed U-values for the uninsulated case capture both ground conduction and internal convection effects, providing a conservative yet sufficiently accurate estimate (e.g. Refs. [16,42,48]).

2.3. Description of reduced-order model for sTES

The sTES model is developed in the open-source Modelica programming language. Modelica's physical modeling approach promotes sTES reproducibility and reusability. In the reduced-order sTES model, components from both low-level libraries (e.g. thermal resistances), and top-level libraries (e.g. energy systems), are integrated. The model's adaptability and compatibility allow for easy integration into broader system models, facilitating detailed simulation of thermal networks employing seasonal thermal energy storage.

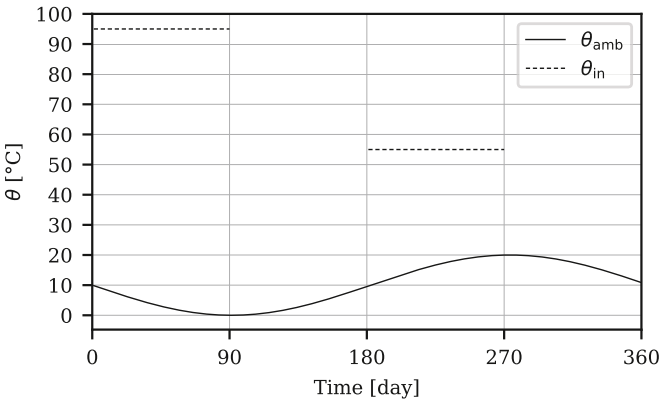

(a) Flow temperatures during one annual cycle and ambient temperatures as a sinus function with an average of 10°C.

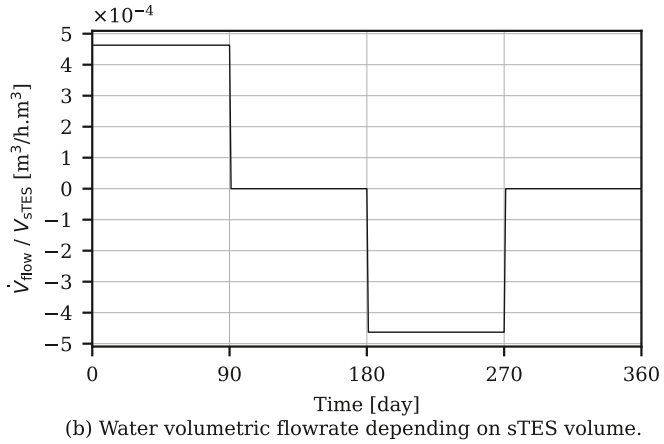

(b) Water volumetric flowrate depending on sTES volume.

Fig. 6. Boundary conditions: A year-round injection flowrate and temperature profiles for the investigated sTES.

2.3.1. Stratified water storage model

The model describes the thermophysical behavior of stratified thermal energy storage systems. It is based on the Modelica Buildings library (*Buildings.Fluid.Storage.BaseClasses.PartialStratified*) [27], with specific modifications to properly represent various geometries, interconnections between segments, and thermal interfaces with the surrounding environment, such as the ground. Fig. 7 illustrates a schematic representation of the sTES model and the ground interaction.

The storage domain is discretized in 1-D into n control volumes in the

Table 1
Design parameters: sTES dimensions of the investigated sizes.

			sTES volume, V [m^3]				
Variable			**20,000**	**50,000**	**100,000**	**150,000**	**200,000**
Top	a, b	[m]	62.5	84.8	108.4	124.0	135.8
Bottom	a_1, b_1	[m]	33.0	45.0	61.6	70.3	75.2
Height	H	[m]	8.5	11.5	13.5	15.5	17.5
Slope	β	[°]	30	30	30	30	30
Surface	A	[m^2]	8,242	15,198	24,724	32,612	38,847
A/V		[m^{-1}]	0.41	0.30	0.25	0.22	0.19

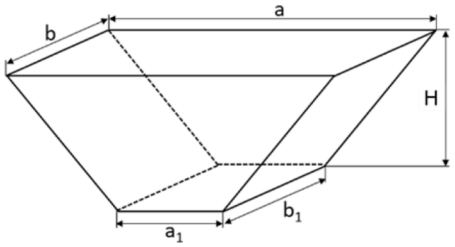

Table 2
Relevant thermo-physical properties and heat transfer coefficients of the different storage components.

Parameter	Symbol	Value	Unit
Water thermal conductivity	λ_w	0.6	W/(m·K)
Water density	ρ_w	998.1	kg/m^3
Water specific heat capacity	$c_{p,w}$	4181	J/(kg·K)
Overall heat transfer coefficient lid	U_{top}	0.1	W/(m^2·K)
Overall heat transfer coefficient side (non-insulated)	U_{side}	90	W/(m^2·K)
Overall heat transfer coefficient bottom (non-insulated)	U_{bot}	90	W/(m^2·K)
Ground thermal conductivity	λ_g	1.8	W/(m·K)
Ground specific heat capacity	$c_{p,g}$	1333	J/(kg·K)
Ground density	ρ_g	2100	kg/m^3
Convective heat transfer coefficient of air	α_c	25	W/(m^2·K)

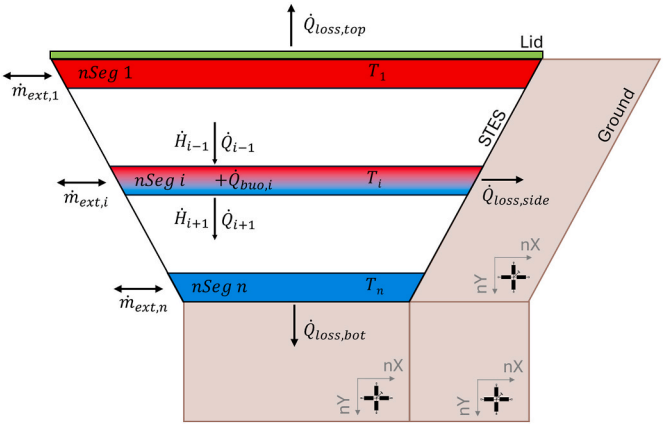

Fig. 7. 2-D representation of the sTES model with surrounding ground and discretization of volume segments.

vertical direction, with equal heights. These segments are connected via fluid ports and heat ports, obeying energy and mass balance constraints. The chosen domain discretization allows the model to describe thermal stratification within the storage, which is maintained via a buoyancy model. The model considers heat losses to the surroundings through the storage walls, lid and bottom, as well as the thermal behavior of the surrounding ground using heat conduction equations. The heat port connections allow the model to calculate heat loss from the storage surface areas (top, sidewalls and bottom), particularly where the storage is in contact with its surrounding. The energy balance in each segment i is governed by:

$$\frac{dE_i}{dt} = \sum \dot{m}_{ext,i} \cdot h_{ext,i} + (\dot{H}_{i-1} - \dot{H}_{i+1}) + (\dot{Q}_{i-1} - \dot{Q}_{i+1}) - \dot{Q}_{loss,i} + \dot{Q}_{buo,i} \quad (1)$$

where $\dot{m}_{ext,i}$ is the mass flow rate entering or leaving the storage at the height of control volume i, $h_{ext,i}$ is the specific enthalpy, $\dot{H}_i$ is the internal enthalpy flow, $\dot{Q}_i$ is the heat conduction between adjacent segments, $\dot{Q}_{loss,i}$ accounts for the lateral heat losses and $\dot{Q}_{buo,i}$ represents the convective heat transport due to buoyancy effects induced by temperature difference along the vertical direction of the storage. The ROM provides full flexibility in defining the number and vertical positions of charging and discharging ports. This enables the simulation of arbitrary inlet/outlet configurations, including multi-port systems. Such configurability allows the model to reflect more realistic and complex PTES operation strategies used in field systems or control optimization studies. The internal enthalpy flows (Equation (2) and Equation (3)) result from the interaction between the upper and lower control volumes and are dependent on the flow direction.

$$\dot{H}_{i-1} = \dot{m}_{i-1} \cdot \begin{cases} h_{i-1} & if\ \dot{m}_{i-1} > 0 \\ h_i & if\ \dot{m}_{i-1} < 0 \end{cases} \quad (2)$$

$$\dot{H}_{i+1} = \dot{m}_{i+1} \cdot \begin{cases} h_i & if\ \dot{m}_{i+1} > 0 \\ h_{i+1} & if\ \dot{m}_{i+1} < 0 \end{cases} \quad (3)$$

The heat flows due to conduction between adjacent elements (cf. Equation (4) and Equation (5)), are determined based on the thermal conductivity of the storage fluid λ_w, the heat transfer area A_i, the distance between fluid nodes Δz_i, and the corresponding temperature difference ΔT_{seg}. The heat conduction and heat loss equations for the TES segments are expressed as follows:

$$\dot{Q}_{i-1} = \lambda_w \cdot \frac{A_{i\ top}}{\Delta z_i} \cdot \Delta T_{seg} \ \left(where\ \Delta T_{seg} = T_{i-1} - T_i\right) \quad (4)$$

$$\dot{Q}_{i+1} = \lambda_w \cdot \frac{A_{i\ bot}}{\Delta z_i} \cdot \Delta T_{seg} \ \left(where\ \Delta T_{seg} = T_i - T_{i+1}\right) \quad (5)$$

The lateral heat losses in Equation (6) are calculated using the overall heat transfer coefficient $U_{wall,i}$, which accounts for both internal convection and the conductive resistance of the wall. The losses also depend on the heat transfer area $A_{wall,i}$, and the temperature difference between the fluid element T_i, and the surrounding $T_{ext,i}$ can refer either to the surrounding air temperature or to the ground element temperature, which is influenced by heat exchange with the TES and the ground's resistance-capacitance model. The lateral heat loss for each segment is given by:

$$\dot{Q}_{loss,i} = \sum U_{wall,i} \cdot A_{wall,i} \cdot \left(T_i - T_{ext,i}\right) \quad (6)$$

Instead of modeling the actual buoyancy-induced volume flow into the adjacent fluid layers, this effect is approximated by introducing a corresponding heat flow rate to the fluid element. The model does not explicitly consider fluid entrainment, as low-turnover rates of seasonal storage result in proportionally low flow velocities, minimizing inlet mixing effects. By inducing heat flow instead of mass flow, the model maintains stratification and prevents unstable thermocline inversions. This upward heat flow can be expressed as [27]:

$$\dot{Q}_{buo,i} = k_{buo} \cdot smooth\left(1, \begin{cases} \Delta T_{seg}{}^2 & if\ \Delta T_{seg} > 0 \\ 0 & if\ \Delta T_{seg} \le 0 \end{cases}\right) \quad (7)$$
$$\left(where\ \Delta T_{seg} = T_{i+1} - T_i\right)$$

$$k_{buo} = V_{i+1} \cdot \rho \cdot c_p \cdot \frac{1}{\tau} \quad (8)$$

where the heat flow $\dot{Q}_{buo,i}$ is governed by the temperature difference, ΔT_{seg}, and the proportionality constant k_{buo}, which relates to the thermal capacity of each segment. This constant k_{buo} is also influenced by a mixing time constant τ. The mixing time constant, τ, controls the rate at which buoyant mixing occurs, with smaller values indicating faster mixing and greater heat transfer rates. The Modelica *smooth(1, expr)* function ensures that the resulting expression is continuously differentiable to first order, to guarantee that the function and its first derivative are continuous.

It should be noted that the internal fluid velocity field and turbulence effects are not explicitly resolved in the simulation. Instead, enthalpic flow between layers are represented through enthalpy transfer governed by the inlet/outlet mass flows and the buoyancy term described above. This buoyancy term is derived based on CFD simulations to capture the role of natural convection that results in decay of stratification. This approach assumes a predominantly laminar and stratified regime within the storage, which is typical for large-volume sTES during idle and slow charging/discharging operations. Therefore, while detailed convective mixing is not resolved, the buoyancy-driven heat exchange term

effectively captures the dominant thermal mixing behavior. This simplification allows for high computational efficiency and is deemed suitable for the model's intended applications in parametric studies, early-stage planning, and real-time system-level simulations.

2.3.1.1. Shape calculation and adaptability. A major advantage of the described sTES model is the ability to handle various sTES geometries, including truncated pyramids, cones, and cylinders, through the so-called *ShapeCalculator*. The focus on a truncated pyramid shape introduces non-uniform segment volumes that more accurately represent real-world sTES systems. For a truncated pyramid, the dimensions of the top (a, b) and bottom (a_1, b_1) layers are interpolated to calculate the segment volumes (Equation (9)) and surface areas (Equation (10)):

$$V_{seg}(i) = \frac{H_{seg}}{6}\left[\left(2\cdot a_{seg} + a_{1\ seg}\right)\cdot b_{seg} + \left(2\cdot a_{1\ seg} + a_{seg}\right)\cdot b_{1\ seg}\right] \tag{9}$$

$$A_{wall\ Seg}(i) = \left(a_{seg} + a_{1\ seg}\right)\cdot\sqrt{\left(\frac{a_{seg} - a_{1\ seg}}{2}\right)^2 + H_{seg}^2} + \left(b_{seg} + b_{1\ seg}\right)\cdot\sqrt{\left(\frac{b_{seg} - b_{1\ seg}}{2}\right)^2 + H_{seg}^2} \tag{10}$$

where H_{seg} is the height of each segment and $a_{seg}, a_{1\ seg}, b_{seg}, b_{1\ seg}$ represent the top and bottom dimensions of each segment. This geometric flexibility enhances model accuracy by enabling variation in segment volumes and associated surface areas across the storage height. This allows more accurate calculation of thermal losses for each layer and simplifies the assignment of boundary conditions that vary by depth or direction (e.g., sidewalls exposed to ambient air vs. soil or adjacent structures), making the model well-suited for complex real-world configurations.

2.3.2. Ground model for TES

The ground model, illustrated in Fig. 8, is implemented as a network of resistance-capacitance (RC) models to describe the thermal response of the ground surrounding the sTES. Each RC-model consists of four resistances and one thermal capacitance (**4R1C**), capturing thermal interactions between the storage and the surrounding ground over time. For each storage wall of the sTES, a 2-D network of ground nodes extends in the vertical and horizontal (away from the wall) directions. **Horizontal resistances** R_{left} and R_{right} are used to describe the heat flow between adjacent elements in the same horizontal layer. **Vertical resistances** R_{top} and R_{bottom} are analogous in the vertical direction. The **heat capacitance** C of each ground element is given by the product of the specific heat capacity and its volume. To improve computational performance, a non-uniform mesh structure is adopted, in which the number of elements along each axis is determined by the sTES's segmentation. Closer to the sTES, mesh elements are thinner to capture steeper temperature gradients, while layers further away are more spaced out, extending up to 50 m (to ensure, that the undisturbed ground temperature won't influence the simulation results) from the sTES. This gradual change in resolution allows for precise simulation near the sTES and efficient computation farther from it. For the comparison, the x-direction was discretized with the first 10 layers set to 2 m width, followed by 3 layers with a width of 10 m. In the y-direction, the ground adjacent to the sTES was set to 10 layers. At the bottom, the first 10 layers have a thickness of 0.5 m, followed by 10 layers at 4.5 m thickness. To ensure thermal coupling between the ground adjacent to the sidewalls and the ground beneath the sTES, an additional mesh region is defined that connects these two domains. This intersecting ground region adopts the vertical resolution of the ground domain below the sTES and the horizontal resolution of the ground domain connected to the sidewalls, resulting in a total of 320 ground elements. This structure balances accuracy with computational efficiency, providing a detailed temperature profile around the sTES and in the surrounding soil.

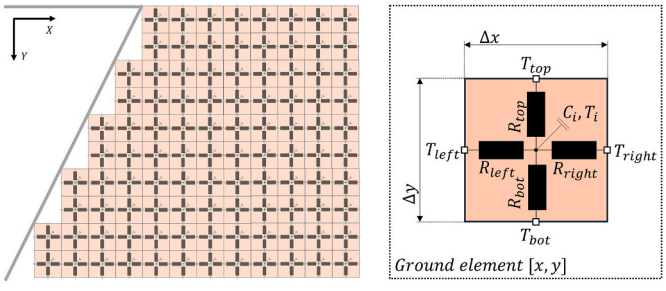

Fig. 8. Ground mesh structure.

The energy balance for each ground element is derived from the 4R1C model, which governs the heat transfer with adjacent elements, the surrounding and heat storage within the element itself. The balance Equation (11) can be expressed as:

$$C_{i[x,y]}\frac{dT_{i[x,y]}}{dt} = \frac{T_{left[x,y]} - T_{i[x,y]}}{R_{left[x,y]}} + \frac{T_{right[x,y]} - T_{i[x,y]}}{R_{right[x,y]}} + \frac{T_{top[x,y]} - T_{i[x,y]}}{R_{top[x,y]}} + \frac{T_{bot[x,y]} - T_{i[x,y]}}{R_{bot[x,y]}} \tag{11}$$

Each thermal resistance R (Equation (12) and Equation (13)) is calculated based on the element's size Δx (width) and Δy (height), as well as the cross-sectional area A perpendicular to each direction of heat flow. Since heat transfer occurs between element centers, Δx and Δy are divided by 2 to represent the half-distance to neighboring elements.

$$R_{left[x,y]} = R_{right[x,y]} = \frac{\Delta x_{[x,y]}}{2\cdot\lambda_g\cdot A_{left/right[x,y]}} \tag{12}$$

$$R_{top[x,y]} = R_{bot[x,y]} = \frac{\Delta y_{[x,y]}}{2\cdot\lambda_g\cdot A_{top/bot[x,y]}} \tag{13}$$

2.4. Key performance indicators

To evaluate the performance and accuracy of the reduced-order sTES model relative to the **validated detailed model**, several KPIs, as listed in Table 3, have been established. The KPIs focus on assessing the accuracy in predicting the dynamic thermal behavior and performance of the storage (e.g. temperatures, heat flows) and on computational efficiency.

The **Root Mean Square Error (RMSE)** is used to assess the accuracy of the model's temperature predictions compared to reference data. RMSE values are calculated at different heights within the sTES, providing a measure of how well the model captures the dynamic temperature behavior during charging and discharging cycles.

Computational time is a performance indicator in evaluating the efficiency of the reduced-order sTES model. It reflects the total time required for the model to complete five annual cycles, providing a measure of the model's practicality and applicability in real-world

Table 3
Key performance indicators for the model comparison during the chosen simulation time.

KPI	Symbol	Unit	Explanation
Charged energy	Q_{ch}	MWh	Energy charged into sTES
Discharged energy	Q_{dc}	MWh	Energy discharged from sTES
Top losses	Q_{top}	MWh	Energy losses through the lid
Side losses	Q_{side}	MWh	Energy losses through the side walls
Bottom losses	Q_{bot}	MWh	Energy losses through the bottom
Total losses	Q_{tot}	MWh	Total energy losses of the sTES
RMSE of temperature	*RMSE*	K	Mean squared error of temperature stratification
Computational time	–	s	Performance indicator of computational efficiency

scenarios. Lower computational time, while maintaining acceptable accuracy, indicates that the reduced-order model is well-suited for large-scale simulations and iterative design processes.

3. Results

To ensure the applicability of the reduced-order sTES model, it is essential to first verify its accuracy in reproducing the system dynamics in shorter simulation time. This verification involves comparing the results of the reduced model with those of *DePlaTES*. The comparison is carried out for ten cases, focusing on the uninsulated scenario, since the uninsulated configuration provides a more challenging and conservative test case for model accuracy, due to stronger ground coupling and consequently increased thermal losses. For the sake of brevity, results are reported only for a selection of five different sizes, where the lid is insulated and the side walls and bottom walls are uninsulated, providing a basis for evaluating the model's thermal predictions.

3.1. Thermal losses

Thermal losses from the sTES, particularly for uninsulated variations, are critical to understanding its energy efficiency. Results shown in Fig. 9 reveal that heat losses through the side walls play a dominant role, especially as the sTES size decreases. For larger sTES, such as the 200,000 m^3 system, side losses Q_{side} account for 53 % of the total annual thermal losses, exceeding 1500 MWh in both models. This dominance of side losses in smaller PTES, such as the 20,000 m^3 volume, is even more pronounced due to the higher surface area-to-volume ratio of 0.16 m^{-1} (A_{wall}/V), where side losses account for approximately 66 % of total losses. Bottom losses Q_{bot} remained the smallest contributor across all sTES sizes, making up less than 9 % of total losses in larger pits (>100,000 m^3) and about 7 % in smaller pits (<100,000 m^3). Despite slight disagreements, particularly in the side losses where discrepancies are limited to 5 %, the overall alignment between the Modelica model and the COMSOL results remains within acceptable range. For instance, in the case of the 200,000 m^3 storage, the deviation in total losses is less than 3 % between both models, corresponding to the values 2928 MWh and 2997 MWh respectively.

The close agreement between both models underscores the reliability of the sTES model in Dymola, approaching the accuracy of the highly detailed COMSOL model under the boundary conditions considered in this work. As the heat losses are highly influenced by the temperature and properties of the surrounding ground, the accuracy of the results suggests that the ground model implemented in Modelica also performs in a similar manner to the detailed COMSOL model. These results validate the Modelica model's ability to accurately predict thermal losses and its potential as a planning tool for large-scale sTES systems. Detailed COMSOL models, on the other hand, offer more flexibility as they can be applied to a wider variety of planning questions (e.g. geometry, role of moisture, groundwater flow), but are less suited for system simulations requiring a short computational time such as those used in digital twins for real-time control and optimization.

3.2. Charged and discharged energy

In sTES systems, it is essential to assess both the charged and discharged energy during annual operations. Fig. 10 and the accompanying Table 4 provide insight into the energy flows for various PTES volumes.

Charged energy values are positive, representing energy supplied to the system, while negative values indicate energy removed from the system. For the largest volume of 200,000 m^3, the comparison shows that the charged energy estimated by the COMSOL model is 9360 MWh, while Dymola estimates a slightly lower value at 8899 MWh, resulting in an absolute deviation of 5.2 %. The discharged energy shows a deviation of 218 MWh, where COMSOL reports −6166 MWh and Dymola −5948 MWh, yielding an absolute deviation of 3.7 %. As the volume decreases, the discrepancies in charged energy values generally decrease. For the 150,000 m^3 case, the charged energy deviation is 4.8 %, which reduces to 3.4 % at 50,000 m^3 and further to 2.4 % at 20,000 m^3. In contrast, discharged energy deviations do not follow a consistent decreasing trend. While the deviation is 3.9 % at 150,000 m^3, it increases slightly to 5.4 % at 50,000 m^3 and then reduces to 5.1 % at 20,000 m^3. Overall, deviations in charged energy between COMSOL and Dymola remain within 2–5 %, with discharged energy deviations ranging between approximately 3.7 % and 5.4 %. This behavior can be attributed to a combination of physical and numerical factors. Smaller storages have a higher surface-to-volume ratio, making thermal losses more dominant and stratification effects less pronounced. In such cases, the ROM's simplified representation of losses and buoyancy-driven flow provides results that align well with the more detailed COMSOL model. In contrast, larger systems develop stronger thermal gradients and more pronounced stratification, especially near the inlets and tank bottom. These effects are sensitive to vertical resolution and local flow modeling. While the COMSOL model captures these behaviors using a fine mesh and fully coupled physics, the ROM employs a simplified, layer-based structure and buoyancy treatment, which can smooth or under-resolve steep gradients. As a result, even small temperature mismatches may accumulate into more noticeable deviations in net charged and discharged energy over long simulation periods in larger storages.

3.3. Deviation in temperature prediction

When comparing the dynamic thermal behavior of the sTES, visible patterns emerge between the two modeling approaches. These

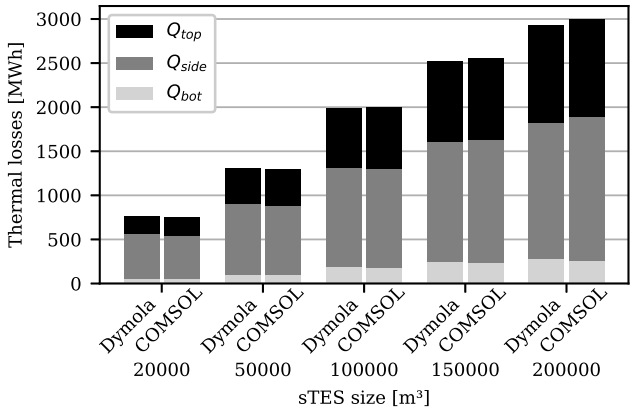

Fig. 9. Comparison of annual thermal losses for both models.

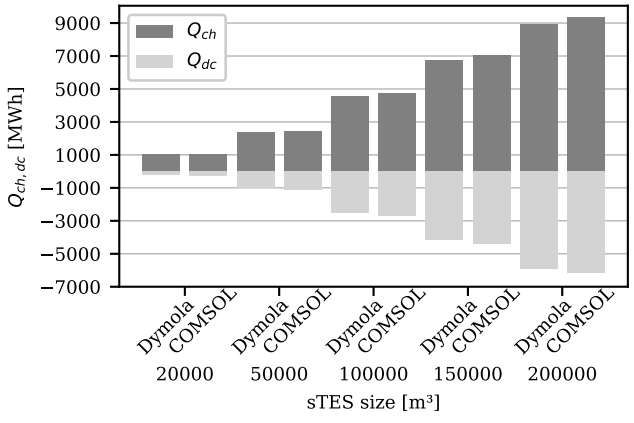

Fig. 10. Charged and discharged energy comparison.

Table 4
sTES energy balance: Thermal losses, charged and discharged energy.

Size [m^3]	Tool	Q_{top} [MWh]	Q_{side} [MWh]	Q_{bot} [MWh]	Q_{tot} [MWh]	Q_{ch} [MWh]	Q_{dc} [MWh]
200,000	COMSOL	1111	1623	263	2997	9360	−6166
	Dymola	1108	1538	279	2925	8899	−5948
	Dev. [%]	−0.3 %	−5.5 %	5.6 %	−2.5 %	−5.2 %	−3.7 %
150,000	COMSOL	922	1397	233	2552	7079	−4386
	Dymola	911	1359	245	2514	6755	−4220
	Dev. [%]	−1.2 %	−2.8 %	4.6 %	−1.5 %	−4.8 %	−3.9 %
100,000	COMSOL	692	1125	177	1994	4773	−2682
	Dymola	678	1127	188	1992	4561	−2554
	Dev. [%]	−2.1 %	0.2 %	5.5 %	−0.1 %	−4.6 %	−5.0 %
50,000	COMSOL	411	792	95	1297	2453	−1110
	Dymola	405	806	101	1311	2372	−1054
	Dev. [%]	−1.5 %	1.7 %	6.1 %	1.1 %	−3.4 %	−5.4 %
20,000	COMSOL	208	496	51	754	1045	−269
	Dymola	203	504	54	762	1021	−256
	Dev. [%]	−2.1 %	1.7 %	6.6 %	1.0 %	−2.4 %	−5.1 %

differences are especially pronounced during dynamic phases, such as transitions between charging and discharging modes, where the temperature profiles clearly diverge. These discrepancies may be attributed to the underlying differences in solver settings and discretization methods employed by each tool. The COMSOL model uses the finite element method, which, depending on the mesh density and the interpolation order within elements, can resolve sharper local features and smooth temperature transitions across regions with steep thermal gradients or rapid inflow dynamics. However, it is important to note that this smoothing is not an inherent feature of FEM itself, but rather a result

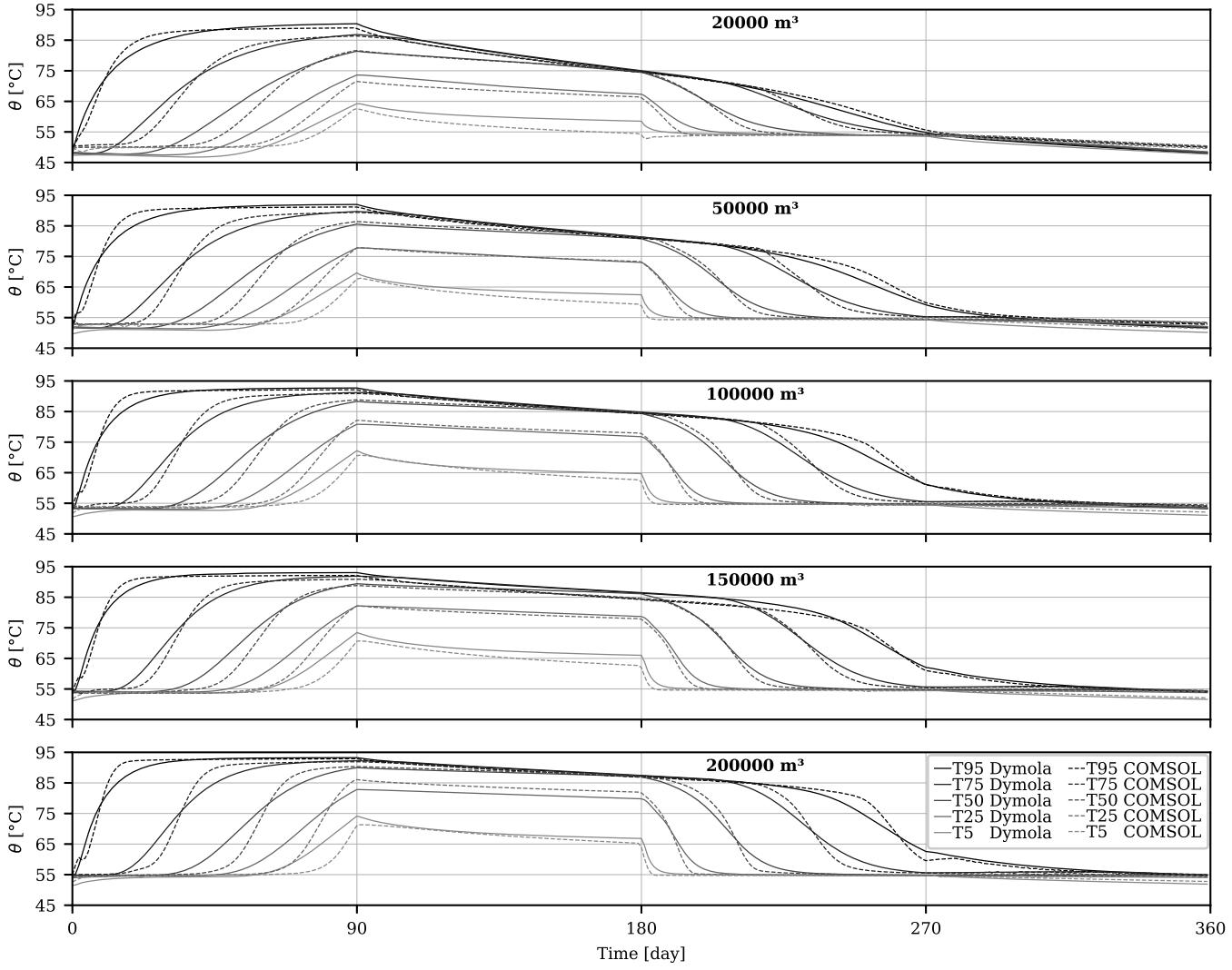

Fig. 11. Temperature stratification profiles at % of the height calculated from the bottom of the storage system. From 95 % near the top (T95) to 5 % near the bottom (T5) of the sTES.

of the chosen discretization and solver configuration. In contrast, the Modelica model applies a finite difference nodal approach, where temperature data is derived from the center of each discretized segment. This leads to more stepwise or dampened transitions, especially in the upper sTES layers during charging, where stratification gradients evolve. The ROM's segment-averaged structure tends to smooth out local fluctuations, resulting in a more uniform but less locally resolved temperature evolution. These relative differences in temperature profiles are particularly evident in regions with rapid thermal changes and are influenced by mesh resolution and flow conditions in both models. While the COMSOL model, with its FEM-based approach, can capture fine-scale variations, the ROM's segment-averaged structure tends to dampen local fluctuations, which in some cases leads to a smoother evolution of temperature gradients.

When comparing the temperature profiles shown in Fig. 11 at different relative heights, the models show close agreement under constant conditions (storage phase and idle phase), particularly at the top layers. When dynamic events occur, the temperature profiles from the two models show minor deviation. During charging, the Modelica model initially underestimates temperatures by up to 3.5 K, especially in the bottom layers, then overestimates by up to 1 K as charging progresses. By the end of the charging phase, the ROM aligns with COMSOL but slightly overestimates peak temperatures. During discharging, the ROM underestimates in the bottom layers and overestimates at the top, converging again in the idle phase. The discrepancy between the models diminishes as one moves toward the top layers, where the predictions over the whole cycle are closely aligned.

To evaluate the prediction accuracy of the ROM compared to the COMSOL model, the RMSE in temperature predictions was calculated at different relative heights within the sTES. As shown in Fig. 12, the RMSE is consistently highest at the bottom of the tank (T5) and decreases steadily toward the top (T95) for all five storage volumes. This trend reflects the stronger thermal gradients and dynamic inflow effects near the base, where modeling deviations are more likely. In contrast, the upper layers exhibit more uniform and slowly varying temperatures, leading to better agreement between models. For example, in the 20,000 m^3 case, the RMSE is approximately 2.4 K at T5 and decreases to about 1.2 K at T95. Across all volumes, average RMSE values remain within a band between 1.4 K and 1.9 K. These results confirm that the ROM captures the key thermal dynamics of the system accurately, especially in upper regions where stratification is stable. The consistent differences near the bottom also explain the deviations in charged and discharged energy discussed in Section 3.2, as these lower layers contribute significantly to the thermal balance. Despite its simplified structure, the ROM shows strong overall agreement with the high-fidelity COMSOL model.

3.4. Computational time

The computational effort of the reduced-order model was evaluated for different sTES sizes on a system with an **Intel(R) Core(TM) i7-1185G7 @ 3.00 GHz** processor and **16 GB of RAM**. Fig. 13 summarizes the computational times for the full simulation of five annual cycles in comparison. Dymola's Dassl-Solver with a tolerance of 1e-06 and a time step between 10 min and 1 day was used for executing the simulations. The ROM was optimized by calibrating the number of vertical segments and configuring solver settings to balance thermal accuracy with simulation speed. The segment count was selected based on convergence tests to ensure stable stratification without excessive runtime. In COMSOL Multiphysics, the direct, fully coupled approach with an adaptive mesh refinement was used, resulting in the application of MUMPS solver with an absolute tolerance of 1e-07 and maximum time stepping restricted to 12 h, whereas the results export had a daily resolution. The ROM reduced the computational time by up to 98 %.

4. Conclusions

The development and validation of a reduced-order model for large-scale PTES has been presented. Implemented in Modelica/Dymola, the reduced-order model exhibits close agreement with a detailed numerical multi-physics model implemented in COMSOL that was previously validated with experimental data from a 60,000 m^3 PTES (Dronninglund pit). The evaluation covered tank sizes ranging from **20,000 m^3 to 200,000 m^3**, with results presented exclusively for **uninsulated configurations** (lid is insulated). This focus reflects the more common real-world use of uninsulated PTES and highlights the critical influence of ground interaction on thermal performance. While insulated configurations were considered during model development, their results are less sensitive to ground heat exchange, making the uninsulated case more relevant for assessing the model's accuracy and robustness. Although the results presented here focused on uninsulated ground configurations, insulated cases were also simulated throughout the course of model development. These configurations revealed further agreement between the ROM and COMSOL DePlaTES model. The insulated results were therefore not shown, since the uninsulated configuration provided a more conservative and demanding benchmark.

The ROM exhibited deviations in annual energy flows within a range of **2 % to 6 %** compared to the detailed COMSOL model. For the largest tank size of **200,000 m^3**, the charged energy deviation was **5.7 %**, while the discharged energy deviation was **4.3 %**. Total thermal losses predicted by the ROM showed a deviation of less than **2 %** across all tested tank sizes. Temperature stratification analysis indicated good agreement under steady-state conditions, particularly in the upper layers of the

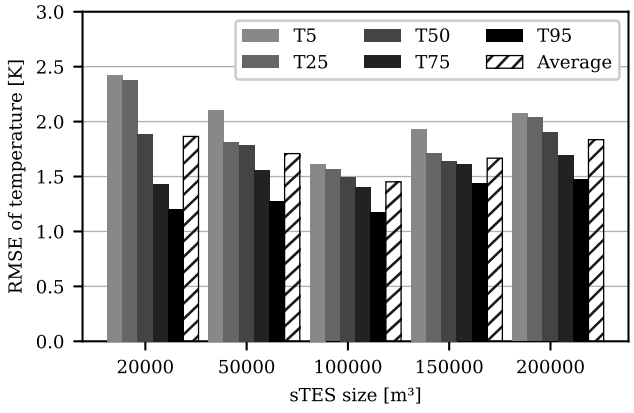

Fig. 12. RMSE of temperature in different relative heights between Dymola and COMSOL.

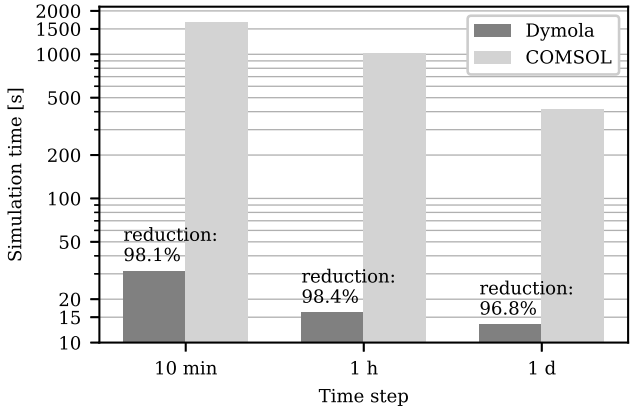

Fig. 13. Simulation time comparison between Dymola and COMSOL Multiphysics.

tank. During dynamic charging and discharging phases, deviations in temperature predictions were more pronounced, but kept below **3 K**. The **RMSE** for temperature predictions ranged from **1.2 K** in the upper layers to **2.4 K** in the bottom layers. In conclusion, the FEM-based approach used in COMSOL allows for more detailed resolution of local gradients, particularly during transient phases and in zones with steep thermal fronts. However, these resolved gradients may appear as non-monotonous transitions or sharp fluctuations in stratification, especially near the inlets and bottom layers. In contrast, the Dymola model, based on a nodal finite difference scheme and coarser vertical segmentation, tends to produce smoother and more continuous temperature profiles due to numerical diffusion and segment-averaging effects. This results in a visually smoother evolution of stratification, particularly in the bottom regions. Although less detailed, this behavior is beneficial in system-level simulations, where computational efficiency and general thermal behavior are prioritized over spatial precision. The different buoyancy formulations applied in each model may further contribute to the stratification deviations observed, but are not analyzed in detail here and will be addressed in future work. Overall, the RMSE analysis shows that while both models perform similarly in most cases, discrepancies in dynamic transitions are more pronounced, particularly during charging phases.

The ROM completed five annual simulation cycles in as little as **13 to 31 s**, depending on the timestep resolution, representing a computational time reduction of up to **98 %** compared to the detailed COMSOL model, demonstrating its suitability for iterative design processes and real-time controls. The ROM's accuracy and efficiency were achieved through iterative model configuration, including the selection of the number of tank layers to adequately capture thermal stratification and employing a calibrated ground mesh to balance precision and efficiency. Finer layers near the tank effectively captured sharper temperature gradients, while coarser layers further from the tank maintained computational speed.

This ROM contributes to sTES modeling and simulation domain by providing a computationally efficient alternative to detailed multi-physics models, which can be used in iterative system design simulation. The ROM enables reliable large-scale sTES in DH system simulations, making it suitable for feasibility studies and development of control strategies in renewable-powered DH networks. While the ROM was seen effective for predicting overall thermal performance, it simplified some transient behaviors, particularly those occurring during highly dynamic charging and discharging phases. The nodal approach in the ROM smoothed the spatial gradients, which might limit its accuracy in capturing transient heat transfer effects compared to the finite element methods used in COMSOL model. Thus, it is crucial to highlight that the ROM application lies fundamentally in system-wide dynamics, while it is not advisable to be used for detailed planning of sTES (e.g. lid heat and moisture transfer).

Future work will focus on further enhancing the model's flexibility and integration potential. Refactoring the model for FMU export could enable its use within broader energy simulation platforms and district heating systems. Expanding the ROM to support different storage media, such as gravel-water mixtures, will increase its applicability across different storage concepts. Additionally, the incorporation of the model within an MPC framework will further enhance its utility in dynamic control and real-time optimization for sustainable energy systems.

While this work focused on comparing the ROM to a high-fidelity COMSOL model, the reduced-order model is currently under validation study considering several datasets from different Danish pit TES systems for multiple operation years (i.e. 2015 up to 2020). This will help to gain further trust in the model when used for system simulations. Future work will report the outcomes of this validation study.

CRediT authorship contribution statement

Michael Bayer: Writing – review & editing, Writing – original draft, Visualization, Validation, Software, Methodology, Investigation, Formal analysis, Data curation, Conceptualization. **Curtis Meister:** Writing – review & editing, Methodology, Conceptualization. **Philipp Schuetz:** Writing – review & editing, Funding acquisition. **Willy Villasmil:** Writing – review & editing, Supervision, Project administration, Funding acquisition. **Heimo Walter:** Writing – review & editing, Supervision. **Abdulrahman Dahash:** Writing – review & editing, Writing – original draft, Visualization, Validation, Software, Investigation, Funding acquisition, Conceptualization.

Declaration of competing interest

The authors declare that they have no known competing financial interests or personal relationships that could have appeared to influence the work reported in this paper.

Acknowledgements

The present study is financially supported by the EU Horizon Europe project INTERSTORES (project No. 101136100). The work has also been supported by the Swiss State Secretariat for Education, Research and Innovation (SERI) (contract No. 23.00535). Views and opinions expressed are however those of the author(s) only and do not necessarily reflect those of the European Union or Research Executive Agency. Neither the European Union nor the granting authority can be held responsible for them.

Data availability

Data will be made available on request.

References

[1] Publications Office of the European Union. A roadmap for moving to a competitive low carbon economy in 2050: communication from the Commission to the European Parliament, the council. the European Economic and Social Committee and the Committee of the Regions; 2011.
[2] Nižetić S, Djilali N, Papadopoulos A, Rodrigues JJPC. Smart technologies for promotion of energy efficiency, utilization of sustainable resources and waste management. J Clean Prod 2019;231:565–91. https://doi.org/10.1016/j.jclepro.2019.04.397.
[3] Ochs F, Dahash A, Tosatto A, Bianchi Janetti M. Techno-economic planning and construction of cost-effective large-scale hot water thermal energy storage for renewable district heating systems. Renew Energy 2020;150:1165–77. https://doi.org/10.1016/J.RENENE.2019.11.017.
[4] International Energy Agency. Directorate of sustainable energy policy. Transition to sustainable buildings: strategies and opportunities to 2050. 2013.
[5] Bott C, Dahash A, Noethen M, Bayer P. Influence of thermal energy storage basins on the subsurface and shallow groundwater. J Energy Storage 2024;92:112222. https://doi.org/10.1016/J.EST.2024.112222.
[6] Sorknæs P. Simulation method for a pit seasonal thermal energy storage system with a heat pump in a district heating system. Energy 2018;152:533–8. https://doi.org/10.1016/j.energy.2018.03.152.
[7] Lindenberger D, Bruckner T, Groscurth HM, Kümmel R. Optimization of solar district heating systems: seasonal storage, heat pumps, and cogeneration. Energy 2000;25:591–608. https://doi.org/10.1016/S0360-5442(99)00082-1.
[8] Xu J, Wang RZ, Li Y. A review of available technologies for seasonal thermal energy storage. Sol Energy 2014;103:610–38. https://doi.org/10.1016/J.SOLENER.2013.06.006.
[9] PlanEnergi. https://planenergi.eu/wp-content/uploads/2023/09/SUNSTORE-3-Phase-2-Implementation.pdf. [Accessed 14 November 2024].
[10] PlanEnergi. SUNSTORE 3 Fase 1 Projektering og udbud 2011. https://energiforskning.dk/files/slutrapporter/slutrapport_incl._bilag_1_12042011_1824.pdf. [Accessed 14 November 2024].
[11] Gabrielli P, Acquilino A, Siri S, Bracco S, Sansavini G, Mazzotti M. Optimization of low-carbon multi-energy systems with seasonal geothermal energy storage: the anergy grid of ETH Zurich. Energy Convers Manag X 2020;8:100052. https://doi.org/10.1016/J.ECMX.2020.100052.
[12] Dahash A, Ochs F, Tosatto A, Streicher W. Toward efficient numerical modeling and analysis of large-scale thermal energy storage for renewable district heating. Appl Energy 2020;279:115840. https://doi.org/10.1016/J.APENERGY.2020.115840.
[13] Formhals J, Kirschstein X, Dahash A, Seib L, Sass I. Development, validation and demonstration of a new modelica pit thermal energy storage model for system simulation and optimization. Geothermal Energy 2024;12:23. https://doi.org/10.1186/s40517-024-00302-9.

[14] Reisenbichler M, Wotawa F, O'Donovan K, Ribas Tugores C, Hengel F. LargeTESModelingToolkit: a modelica library for Large-scaleThermal energy storage modeling and simulation. In: Dirk Müller, Antonello Monti, Andrea Benigni, editors. Proceedings of the 15th international modelica conference; 2023, 2023. p. 334–46. https://doi.org/10.3384/ecp204.
[15] Dahash A, Ochs F, Tosatto A. Techno-economic and exergy analysis of tank and pit thermal energy storage for renewables district heating systems. Renew Energy 2021;180:1358–79. https://doi.org/10.1016/J.RENENE.2021.08.106.
[16] Dahash A, Ochs F, Tosatto A. Developments in simulation and evaluation of large-scale hot water tanks and pits in renewables-based district heating. 2021. https://doi.org/10.26868/25222708.2021.30259.
[17] Dahash A, Ochs F, Tosatto A. Techno-economic planning and exergy analysis of large-scale hot-water tank and pits. 2022. https://doi.org/10.2991/ahe.k.220301.008.
[18] Dahash A, Ochs F, Janetti MB, Streicher W. Advances in seasonal thermal energy storage for solar district heating applications: a critical review on large-scale hot-water tank and pit thermal energy storage systems. Appl Energy 2019;239:296–315. https://doi.org/10.1016/J.APENERGY.2019.01.189.
[19] University of Wisconsin SEL. TRNSYS 17: A transient system simulation program 2012 [software], http://www.trnsys.com.
[20] Raab S, Mangold D, Müller-Steinhagen H. Validation of a computer model for solar assisted district heating systems with seasonal hot water heat Store. Sol Energy 2005;79:531–43. https://doi.org/10.1016/J.SOLENER.2004.10.014.
[21] Li X, Wang Z, Li J, Yang M, Yuan G, Bai Y, et al. Comparison of control strategies for a solar heating system with underground pit seasonal storage in the non-heating season. J Energy Storage 2019;26:100963. https://doi.org/10.1016/J.EST.2019.100963.
[22] Bai Y, Wang Z, Fan J, Yang M, Li X, Chen L, et al. Numerical and experimental study of an underground water pit for seasonal heat storage. Renew Energy 2020;150:487–508. https://doi.org/10.1016/J.RENENE.2019.12.080.
[23] Bai Y, Yang M, Fan J, Li X, Chen L, Yuan G, et al. Influence of geometry on the thermal performance of water pit seasonal heat storages for solar district heating. Build Simul 2021;14:579–99. https://doi.org/10.1007/s12273-020-0671-9.
[24] Xie Z, Xiang Y, Wang D, Kusyy O, Kong W, Furbo S, et al. Numerical investigations of long-term thermal performance of a large water pit heat storage. Sol Energy 2021;224:808–22. https://doi.org/10.1016/J.SOLENER.2021.06.027.
[25] Klöck M. Validierung eines Simulationsmodells für solare Fernwärmeversorgungen mit saisonalem Erdbecken-Wärmespeicher. Steinbeis Forschungsinstitut für solar e und zukunftsfähige thermische Energiesysteme, Reutlingen: hochschul e Reutlingen. 2018.
[26] Gauthier G. Benchmarking, and improving models of subsurface heat storage dynamics: comparison of Danish PTES and BTES installation measurements with their corresponding TRNSYS models. GEOTHERMICA – ERA NET Cofund Geothermal 2020:47.
[27] Wetter M, Zuo W, Nouidui TS, Pang X. Modelica buildings library. J Build Perform Simul 2014;7:253–70. https://doi.org/10.1080/19401493.2013.765506.
[28] Jorissen F, Reynders G, Baetens R, Picard D, Saelens D, Helsen L. Implementation and verification of the IDEAS building energy simulation library. J Build Perform Simul 2018;11:669–88. https://doi.org/10.1080/19401493.2018.1428361.
[29] Müller D, Lauster M, Constantin A, Fuchs M, Remmen P. AixLib – an open-source modelica library within the iea-ebc annex 60 framework. Proceedings CESBP - Central European Symposium on Building Physics/BauSIM 2016 2016;6:3–9.
[30] Nytsch-Geusen C, Huber J, Ljubijankic M, Rädler J. Modelica BuildingSystems – eine Modellbibliothek zur Simulation komplexer energietechnischer Gebäudesysteme. Bauphysik 2013;35:21–9. https://doi.org/10.1002/BAPI.201310045.
[31] Graber M, Kosowski K, Richter C, Tegethoff W. Modelling of heat pumps with an object-oriented model library for thermodynamic systems. Math Comput Model Dyn Syst 2010;16(3):195–209. https://doi.org/10.1080/13873954.2010.506799.
[32] Graber M, Kosowski K, Richter C, Tegethoff W. Modelling of heat pumps with an object-oriented model library for thermodynamic systems. Proceedings Mathmod 2009. https://doi.org/10.1080/13873954.2010.506799.
[33] TLK Thermo GmbH. TIL – Model library for thermal components and systems. https://www.tlk-thermo.com/index.php/en/til-suite.
[34] TLK Thermo GmbH. TILMedia – Model library providing thermophysical properties https://www.tlk-thermo.com/index.php/en/til-suite..
[35] Hoppe T, Braune J, Nielsen L. Dynamic system simulation for new energy markets - optimization of a coal fired power plant startup procedure. VGB PowerTech 2019:47–51. https://www.vgbe.energy/wp-content/uploads/2020/04/VGB-POWERTECH-2019-09-047-051-HOPPE-Specimen-Copy.pdf. [Accessed 14 November 2024].
[36] Köfinger M, Schmidt RR, Basciotti D, Terreros O, Baldvinsson I, Mayrhofer J, et al. Simulation based evaluation of large scale waste heat utilization in urban district heating networks: optimized integration and operation of a seasonal storage. Energy 2018;159:1161–74. https://doi.org/10.1016/J.ENERGY.2018.06.192.
[37] Dahash A, Ochs F, Tosatto A. Simulation-based design optimization of large-scale seasonal thermal energy storage in renewable-based district heating systems. In: Proceedings of BauSIM 2020 (virtual): 8Th conference of IBPSA Germany and Austria; 2020. https://doi.org/10.3217/978-3-85125-786-1. Graz, Austria.
[38] Reisenbichler M, O'Donovan K, Ribas Tugores C, van Helden W, Wotawa F. Towards more efficient modeling and simulation of large-scale thermal energy storages in future local and district. Energy Systems 2021. https://doi.org/10.26868/25222708.2021.30911.
[39] Bott C, Ehrenwirth M, Trinkl C, Bayer P. Component-based modeling of ground-coupled seasonal thermal energy storages. Appl Therm Eng 2022;214:118810. https://doi.org/10.1016/J.APPLTHERMALENG.2022.118810.
[40] Solar-Institut Juelich. CARNOT toolbox, ver. 7.0, 07/2019 for matlab/simulink R2018b n.d. https://fh824aachen.sciebo.de/index.php/s/0hxub0iIJrui3ED?path=%2FCARNOT_documentation_7.0. [Accessed 14 November 2024].
[41] Dahash A, Bianchi Janetti M, Ochs F. Detailed axial symmetrical model of large-scale underground thermal energy storage. In: Proceedings of the 2018 COMSOL conference; 2018. Lausanne, Switzerland.
[42] Dahash A, Ochs F, Giuliani G, Tosatto A. Understanding the interaction between groundwater and large-scale underground hot-water tanks and pits. Sustain Cities Soc 2021;71:102928. https://doi.org/10.1016/J.SCS.2021.102928.
[43] Feflow DHIA/S. Subsurface flow & transport modeling n.d. https://www.dhigroup.com/technologies/mikepoweredbydhi/feflow. [Accessed 14 November 2024].
[44] Tosatto A, Dahash A, Ochs F. Simulation-based performance evaluation of large-scale thermal energy storage coupled with heat pump in district heating systems. J Energy Storage 2023;61:106721. https://doi.org/10.1016/J.EST.2023.106721.
[45] Salvestroni M, Pierucci G, Pourreza A, Fagioli F, Taddei F, Messeri M, et al. Design of a solar district heating system with seasonal storage in Italy. Appl Therm Eng 2021;197:117438. https://doi.org/10.1016/J.APPLTHERMALENG.2021.117438.
[46] EDSL USA Inc. Tas: fast and robust Building Simulation Software [software] https://www.edsltas.com..
[47] Dahash A, Ochs F, Bianchi Janetti M, Streicher W. Advances in seasonal thermal energy storage for solar district heating applications: a critical review on large-scale hot-water tank and pit thermal energy storage systems. Appl Energy 2019;239:296–315. https://doi.org/10.1016/j.apenergy.2019.01.189.
[48] Gao M, Shao S, Xiang Y, Wang D, Furbo S, Fan J. Semi-analytical model of a large-scale water pit heat storage for the long-term thermal applications. Energy Build 2024;307. https://doi.org/10.1016/j.enbuild.2024.113975.